Scaling of Repeating Earthquakes at the Transition From Aseismic to Seismic Slip

Olivier Lengliné, Jean Paul Ampuero, Jean Schmittbuhl

AGU ADVANCING EARTH AND SPACE SCIENCE

Geophysical Research Letters®

RESEARCH LETTER
10.1029/2022GL101604

Scaling of Repeating Earthquakes at the Transition From Aseismic to Seismic Slip

O. Lengliné[1], J. P. Ampuero[2], and J. Schmittbuhl[1]

[1]EOST/ITES, Université de Strasbourg/CNRS, Strasbourg, France, [2]Université Côte d'Azur, IRD, CNRS, Observatoire de la Côte d'Azur, Géoazur, Valbonne, France

Key Points:

- Effective normal stress influences the properties of repeating earthquakes in a rate-and-state friction model
- Fluctuations of effective normal stress reproduce the unusual scaling between moment and rupture size of repeating earthquakes
- Non self-similar scaling is an indicator of proximity to the transition between the seismic and aseismic slip

Supporting Information:

Supporting Information may be found in the online version of this article.

Correspondence to:

O. Lengliné,
lengline@unistra.fr

Citation:

Lengliné, O., Ampuero, J. P., & Schmittbuhl, J. (2023). Scaling of repeating earthquakes at the transition from aseismic to seismic slip. *Geophysical Research Letters*, *50*, e2022GL101604. https://doi.org/10.1029/2022GL101604

Received 5 OCT 2022
Accepted 12 FEB 2023

Abstract Some observations of repeating earthquakes show an unusual, non-self-similar scaling between seismic moment and corner frequency, a source property related to rupture size. These observations have been mostly reported in regions at the transition from stable to unstable slip, in geothermal reservoirs and subduction zones. What controls the non self-similarity of these ruptures and how this is linked to the frictional stability of the interface are still open questions. Here we develop seismic cycle simulations of a single unstable slipping patch to investigate the mechanisms underlying this behavior. We show that temporal changes of normal stress on a fault can produce ruptures that exhibit the observed anomalous scaling. Our results highlight the role of fault zone fluid pressure in modulating the effective normal stress and contributing to the sliding stability of the fault.

Plain Language Summary The observation that some earthquakes have nearly similar source lengths but the varying magnitude is at odds with empirical earthquake scaling relations observed worldwide. Here we test how the influence of fluid pressure (or, equivalently, effective normal stress) on the fault could explain atypical size-duration scaling. We run numerical simulations of a fault containing an asperity that can produce repeating earthquakes. We observe that this asperity can slip seismically or aseismically depending on the value of the effective normal stress imposed on the fault. For a given asperity size, there exists a range of effective normal stress that leads to earthquakes with quasi identical lengths but strongly varying magnitudes. The relation between these two quantities is close to the one observed for these atypical earthquakes on natural faults. We thus propose that an explanation for anomalous size-duration scaling can be related to the fluctuations of fluid pressure within a fault.

1. Introduction

The increase of pore-pressure in fault zones has been linked in many instances to the occurrence of earthquakes (e.g., Lengliné et al., 2017; Miller, 2013). This is mainly explained by the resulting decrease in effective normal stress bringing the fault closer to frictional failure (Gischig, 2015). Slip on faults that reach failure is then responsible for induced earthquakes. However, the onset of slip does not imply slip is unstable: it could become seismic or stay aseismic, that is, having high or low rupture speed, respectively, compared to seismic wave speeds. Indeed, in numerous instances the increase of pore pressure in seismogenic faults has been suggested to promote aseismic slip, such as in geothermal reservoirs (e.g., Cornet et al., 1997), in controlled experiments at various scales (De Barros et al., 2018; Passelègue et al., 2020), in crustal rift zones (De Barros et al., 2020) or subduction interfaces (Warren-Smith et al., 2019). Induced aseismic slip often goes along with repeating seismic signals interpreted as radiated by the rupture of seismic patches embedded in an otherwise creeping fault. Such repeating signals have been observed in various contexts, including geothermal reservoirs (e.g., Bourouis & Bernard, 2007) or subduction zones, where they take the form of low frequency earthquakes (e.g., Frank et al., 2015). The analysis of these repeating earthquakes has revealed an intriguing behavior: the relation between their corner frequency, f_c (generally interpreted in terms of characteristic rupture length, l), and their seismic moment, M_0, does not follow the typical scaling law (Bostock et al., 2015; Bouchon et al., 2011; Cauchie et al., 2020; Farge et al., 2020; Harrington & Brodsky, 2009; Lengliné et al., 2014; Lin et al., 2016). Indeed, in these examples it was observed that the moment can span nearly two orders of magnitude while the rupture length varies only weakly. This is at odds with the scaling $M_0 \propto \Delta\sigma l^3$, where $\Delta\sigma$ is the stress drop, inferred for most earthquakes worldwide and classically associated with self-similar rupture models (e.g., Duputel et al., 2013). However, this equation also shows that a repeating earthquake sequence that satisfies the self-similar scaling with almost constant l but variable $\Delta\sigma$ could explain the atypical observation qualitatively. There exist several factors that can influence the

stress drop of an earthquake, one notable one would be a change in loading rate. However changing the loading rate produces mostly a change of l and a modest variation of M_0 which is not consistent with the reported observations (Chaves et al., 2020; Vidale et al., 1994) (See Figure S1 in Supporting Information S1). Changing $\Delta\sigma$ by changing fluid pressure is another possible scenario, which we consider here. We further use a numerical modeling approach to reproduce quantitative aspects of the anomalous source scaling observations. In particular, we investigate how a pore pressure perturbation on a fault can modify the nucleation of micro-earthquakes and the proportion of aseismic slip. We analyze the variations of the source parameters of the simulated seismic events as a function of the effective normal stress perturbation. We find that the abnormal scaling relation can emerge from distinct pore pressure conditions and is quantitatively explained by the model.

2. Model

2.1. A Rate-And-State Friction Model

In earthquake cycle models, the equations governing slip on a fault are often modeled assuming rate-and-state state friction (Dieterich, 1992). We follow that framework and describe the modeling equations in Text S1 in Supporting Information S1. Under this model assumption, the stability of slip is governed by the balance between the shear stress imposed on the fault and the frictional strength. In a 1D spring slider model, unstable slip occurs when the rigidity of the medium, k, is higher than a critical rigidity (Scholz, 1998),

$$k^* = \frac{(b-a)\sigma_n^{\text{eff}}}{D_c}, \tag{1}$$

where a and b are rate-and-state friction parameters that control the response of the friction coefficient to a change of slip velocity and of fault state variable, respectively, D_c is a characteristic slip distance for the evolution of the state variable, and $\sigma_n^{\text{eff}} = \sigma_n - P_p$ is the effective normal stress on the fault. No spontaneous instability occurs if $(b-a) < 0$, that is, if the fault is velocity-strengthening at a steady state. If σ_n^{eff} decreases then k^* decreases and the fault is less prone to unstable sliding. The rigidity of a locked circular patch of radius L on a plane driven by a remote stress is

$$k = \frac{G}{2L} \tag{2}$$

where G is the shear modulus of the elastic medium (Ampuero & Rubin, 2008). Combining Equations (1) and (2) gives the minimum size of the circular patch for nucleation of an instability

$$L_c = \frac{D_c G}{2(b-a)\sigma_n^{\text{eff}}}. \tag{3}$$

A decrease in the effective normal stress causes an increase of L_c. Thus, increasing the pore-pressure on a fault may stabilize its seismogenic patches and turn them into aseismic patches. It may also lead to an intermediate behavior in which seismogenic patches become subdued seismic patches, producing earthquakes with smaller moments compared to their unperturbed pore-pressure state. Here we investigate these intermediate cases with the help of a numerical model.

2.2. Modeling the Fault

We consider a quasi-dynamic numerical model of a fault governed by rate-and-state friction (Luo & Ampuero, 2018; Luo et al., 2017), as described in Text S1 in Supporting Information S1. We investigate a simple model of 1D straight fault embedded in a 2D elastic medium, driven by a far field loading and slipping in the anti-plane direction. While there might be quantitative differences between quasi-dynamic and fully-dynamic models (Thomas et al., 2014), we consider that the dynamic stress changes carried by seismic waves will not modify the results obtained here because we focus on isolated asperities with simple geometry. Moreover, we are mostly interested in the variation of observed parameters rather than in their absolute values, such that our approximate representation of co-seismic stress transfer should not impact the observed relative trends. We consider an asperity described as a potentially unstable patch with $a < b$. The rate-and-state friction properties a, b, and D_c are assumed constant and independent of pore-pressure. While such a dependency is possible, as

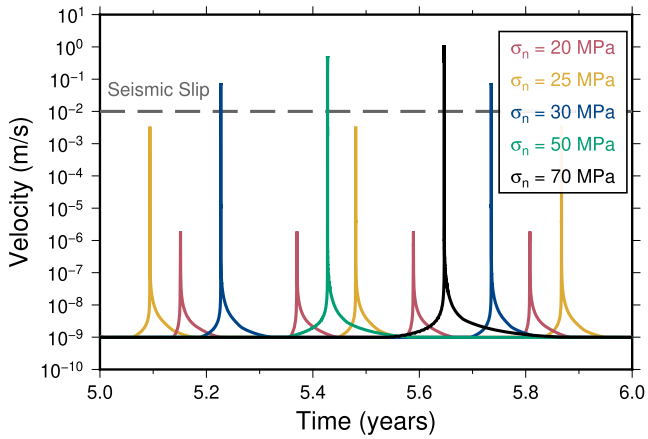

Figure 1. Examples of maximum slip rate evolution for a fault model of length $L_x = 1{,}000$ m, an asperity of half-size $R = 100$ m driven by a constant loading rate, $V_l = 10^{-9}$ m.s^{-1}. Each curve results from a different simulation with a different normal stress (see legend). The gray dashed line indicates the threshold slip rate, v_{th}, used here to define seismic slip.

reported by Scuderi and Collettini (2016), we hypothesize that its effect on the fault shear strength is small compared to the linear dependence of shear strength on pore pressure via the effective normal stress.

We adopt similar properties of the fault and of the nucleation patch as Chen and Lapusta (2009) except that we consider a 1D fault. The elastic medium has a shear modulus $G = 30$ GPa and the far field loading velocity is $V_l = 10^{-9}$ m/s. The fault has a steady state friction coefficient $\mu_{ss} = 0.6$ at the sliding velocity of $V_{ss} = V_l$. We also run simulations with a higher shear modulus ($G = 45$ GPa), keeping all other parameters constant, and obtain a similar conclusion (See Text S2 and Figure S3 in Supporting Information S1). A velocity-weakening patch of length L lies in the middle of the fault with $a = 0.015$ and $b = 0.019$. Outside this patch, we consider a velocity strengthening zone with $a = 0.019$ and $b = 0.015$. The total modeled domain has a length of $L_x = 1{,}000$ m and outside the domain, we impose stable sliding at the plate velocity. The critical slip distance, D_c, is set to 160 μm. We do the simulations with the boundary element software QDYN (Luo et al., 2017). The fault is decomposed into $N = 1024$ elements. The element size, $dx = L_x/N$, is between 3 and 16 times smaller than the process zone size $L_b = GD_c/b\sigma_{\text{eff}}$ for the range of values of σ_{eff} we considered, ensuring that the numerical model has a proper spatial resolution. To avoid the influence of the initial conditions, we only considered the results after several earthquake cycles have occurred. Each simulation is performed under temporally constant and spatially uniform normal stress. We systematically study the influence of the normal stress on the sliding stability of seismic fault patches of different sizes L.

3. Results

We first consider a velocity weakening region of half-size $R = L/2 = 100$ m. We run several simulations by imposing various values of the effective normal stress (typically between 20 and 200 MPa) which are representative of the conditions of an earthquake in the shallow crust. We show in Supporting Information S1 (Text S3, Figure S4 and Tables S1 and S2 in Supporting Information S1) that the alternative approach of applying a step in σ_n at some time within a repeating earthquake cycle and looking at the properties of the next rupture that immediately follows this step change, leads to similar results as those presented here. Under constant normal stress and constant remote loading rate, the velocity-weakening patch may experience phases of slip acceleration (instabilities). We track the evolution of the maximum slip velocity in Figure 1. It remains close to the loading velocity most of the time, punctuated by transient increases in slip rate. These transients only occur for sufficiently large normal stress. Below this normal stress threshold, the simulated fault is stable and no instability developed. We define $v_{th} = 1$ cm/s as the velocity threshold separating aseismic from seismic slip, as in previous studies (e.g., Chen & Lapusta, 2009). When the normal stress is too low the slip rate remains lower than v_{th}; we then consider that all the slip on the asperity, even during the slip event, is aseismic. We observe that the maximum slip speed increases with increasing normal stress and exceeds v_{th} when σ_n becomes larger than about 30 MPa. The results of Rubin and Ampuero (2005) suggest that, for an antiplane rupture, the minimum normal stress required to cause seismic slip on a velocity-weakening patch of half-size R is

$$\sigma_n = \frac{2GbD_c}{\pi(b-a)^2 R}, \tag{4}$$

Given our parameters values, we have $\sigma_n = 36$ MPa, close to the observed value. For higher values of normal stress, the maximum slip velocity remains around 1 m/s. Therefore, there exists a minimum normal stress value above which seismically detectable events exist (Figure 1). Such prediction is a well known behavior of the rate-and-state friction model, in which the slip behavior of an isolated asperity is controlled by the ratio between the nucleation length defined by Rubin and Ampuero (2005) and the patch length (Barbot, 2019; Rubin, 2008).

We now document how the seismic moment evolves when the normal stress changes during seismic cycles. We determine the starting time, t_s, and ending time, t_e, of each seismic event as the times when the maximum slip rate becomes larger than and lower than v_{th}, respectively. For each event, we compute the distribution of co-seismic slip, D, as a function of the distance to the center of the asperity, x_i, as

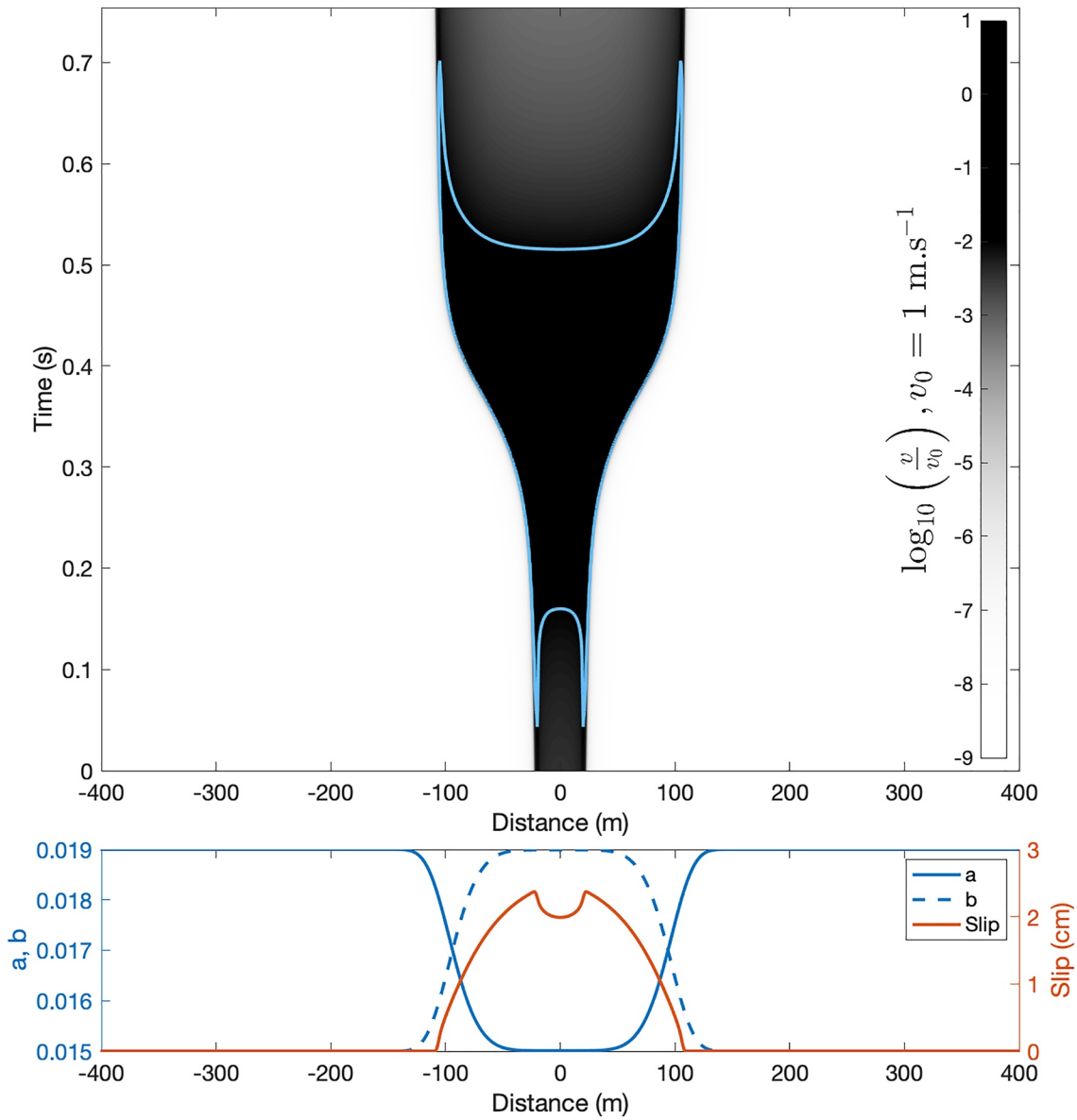

Figure 2. Top: Slip rate as a function of time, t and distance along fault, x during a simulated earthquake (grayshade). Slip rate higher than v_{th}, indicating a seismic rupture, is highlighted with the blue contour interval. The simulation is performed for $R = 100$ m and $\sigma_n = 50$ MPa (Slip velocity contours for other normal stresses are represented in Figure S2 in Supporting Information S1). Bottom: Values of the a and b parameters of the friction law along the fault (solid and dashed blue lines). The seismic slip profile, $D(x)$ computed for this rupture is shown in orange. We extract the length of the seismic rupture from this profile as the maximum position along the fault where $D(x)$ is non-zero which in this example is around 106 m.

$$D(x_i) = \sum_{\substack{t=t_s \\ v(t,x_i) > v_{th}}}^{t_f} u(x_i, t) \tag{5}$$

where $u(x_i, t)$ and $v(x_i, t)$ are, respectively, the slip and the slip rate computed along the fault at position x_i and at time t (see Figure 2). The position x_i varies from $-L_x/2$ to $L_x/2$ in N steps dx. We convert this distribution of slip from an 1D fault to slip on a (2D) fault plane following the approach of (Lapusta & Rice, 2003; Rubin & Ampuero, 2005) which assumes a radial symmetry of the slip profile, centered at the middle of the asperity, such that the seismic potency, P_0, is computed as

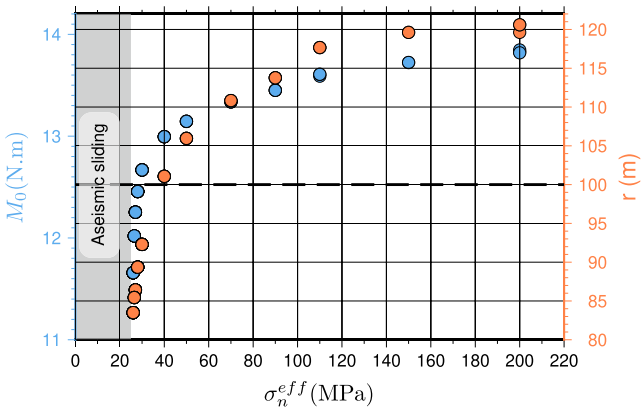

Figure 3. Variation of the moment, M_0 (blue circles) and the rupture length, r (orange circles) for simulation of a seismic patch with $R = 100$ m (denoted by a black dashed line) as a function of the effective normal stress. For a fault with low normal stress below 30 MPa, slip remains aseismic.

$$P_0 = 2\pi \sum_{x_i=0}^{L_x/2} D(x_i) x_i dx. \quad (6)$$

Finally, the seismic moment is obtained from $M_0 = GP_0$.

We report in Figure 3 the evolution of the seismic moment, M_0 as a function of the effective normal stress, σ_n. From the aseismic/seismic transition up to the maximum achieved seismic moment, M_0 increases by two orders of magnitude. Thus the same asperity can produce earthquakes with various seismic moments depending on their normal stress. We also report on the same figure the rupture size of seismic events, r. We simply consider that $r = \max(x)|v(x,t) > v_{th}, t \in [t_s; t_e]$. We observe that r grows monotonically with the effective normal stress. The rupture size is either smaller than the seismic patch (velocity weakening zone) or larger by penetrating into the velocity-strengthening zone. The values of r are distributed around the values of the half-size of the unstable patch, R, and typically vary over a range of $\pm 20\%$. Both values of r and M_0 grow rapidly after the aseismic/seismic transition and then flatten as the normal stress is increased.

To document how this observation translates at the moment versus radius scaling of earthquakes, we run simulations with different asperity radii ($R = L/2 = 30$, 70, 100, and 300 m) and, for each simulation, we extract the seismic moment and rupture size of each event when varying the normal stress (from 20 to 110 MPa). For simulations performed with $R = 300$ m, we increased the total modeled domain to a length of 2,000 m and the number of elements to 2048. We show in Figure 4 the scaling of the moment versus rupture size. We observe that, globally, all results fall within the typical scaling

$$M_0 = \frac{7}{16} \Delta\sigma r^3 \quad (7)$$

where $\Delta\sigma$ is the stress drop of a circular crack model (Eshelby, 1957). The range of stress drops identified in Figure 4 varies over two orders of magnitude, between 1 and 100 MPa. The lowest stress drops are observed for the lowest values of normal stress and, as the normal stress increases, so does the stress drop, as previously observed by Kato (2012). As expected from Equation 4, for a given asperity size, R, a seismic rupture is only observed for a sufficiently high normal stress. Below this value, the rupture is entirely aseismic (based on our definition). We note that the smaller size earthquakes need only a slight decrease of normal stress to undergo a profound variation

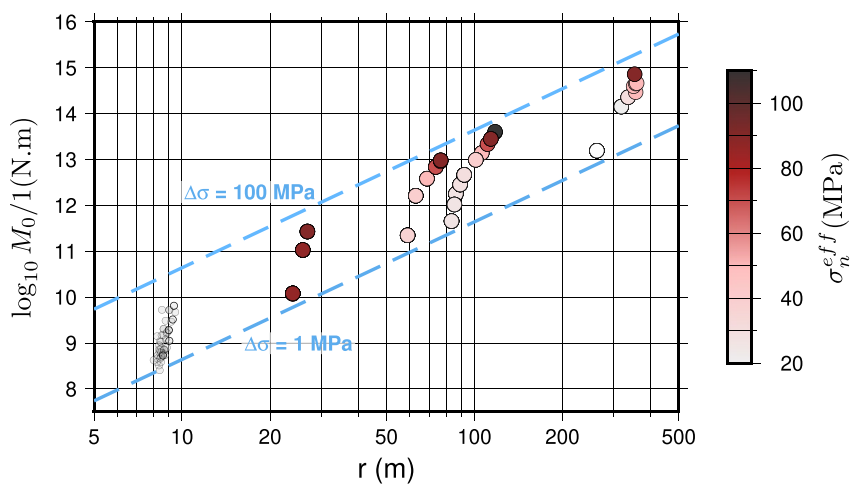

Figure 4. Moment, M_0 as a function of the rupture size, r computed for four asperity sizes, R (colored circles). The color of each circle refers to the normal stress used during each simulation. The dashed blue lines indicate the scaling $M_0 \propto r^3$ considering a stress drop of one or 100 MPa. The gray transparent dots show the scaling of a repeating earthquake sequence identify in Cauchie et al. (2020) for comparison.

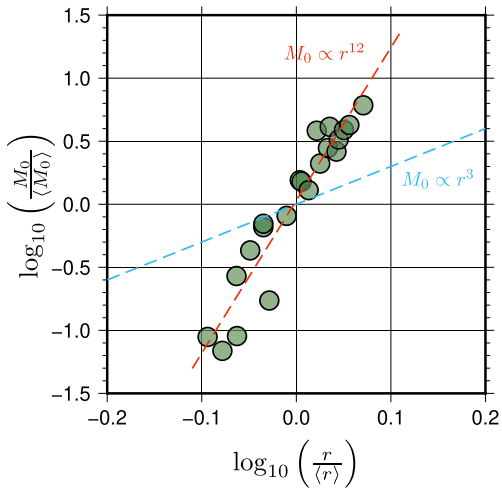

Figure 5. Normalized moment as a function of the normalized rupture length (green dots). This shows the scaling between moment and rupture size within a repeating sequence. The blue dashed line shows the typical $M_0 \propto r^3$ scaling while the red dashed line shows the best fit to the data highlighting a significantly different scaling.

of stress drop, while for larger ruptures the change of normal stress required to produce the same effect is more important. This suggests that the effect of normal stress is mainly visible in the smaller ruptures.

For a given seismic patch or asperity size, the scaling between moment and rupture size appears to depart from Equation 7, showing a sharp increase of moment with rupture size. We document this scaling of the moment with rupture size within a seismic patch (i.e., a repeating earthquake sequence corresponding to a set of events with a similar asperity size but various prescribed values of normal stress). To reveal this connection, we compute for each of the four seismic patch sizes, R, the normalized moment, $M_0/\langle M_0\rangle$, and the normalized rupture size, $r/\langle r\rangle$, normalizing by their mean values. Despite some scatter, the two orders of magnitude variation of the normalized moment are retrieved while the variation of the normalized rupture size is small (Figure 5). These results clearly indicate that for repeating ruptures on a seismic patch with varying normal stress, a moment - size scaling emerges with an exponent much higher than the value of three expected from self-similarity. A linear least squares regression between the logarithm of the normalized moment and the logarithm of the normalized rupture size reveals that the two quantities are well related by a linear relation with a slope of 12 (Figure 5). We acknowledge however that a power law model is of limited quality due to the very small range of normalized rupture size and one could also consider other forms of laws to fit these data. However, we assume this power-law expression as it is the one reported in studies on natural cases (Bostock et al., 2015; Cauchie et al., 2020; Farge et al., 2020; Harrington & Brodsky, 2009).

4. Discussion

Our results can be compared to observations from active faults. For example, Bostock et al. (2015) resolve a similar scaling as in Figure 5 linking the corner frequency to the moment of low frequency earthquakes in the Cascadia subduction zone. Assuming the corner frequency is inversely proportional to the rupture length, as in classical earthquake source models (Savage, 1972), the moment - size exponent for the low frequency earthquakes in Cascadia is around 10. Similarly, Farge et al. (2020) resolve such an anomalous scaling for low frequency earthquakes in the Mexican subduction zone with an exponent between 8 and 19 depending on the method used. In the Soulz-sous-Forêts geothermal area, Cauchie et al. (2020) show that the scaling relation within repeating earthquake families exhibits a similar scaling with an exponent close to 20 (see Figure 4 for an example). For earthquakes on the San-Andreas fault at Parkfield, Harrington and Brodsky (2009) get an exponent of 17.

All these observations show that for a single family the seismic moment varies at most over two orders of magnitude. Our simulation results are in good agreement with these reported observations and thus constitute a possible explanation for this observed anomalous scaling. We note that our observations are not necessarily in contradiction with the self-similar scaling of LFE as reported for example, by Supino et al. (2020). Indeed, in their study, Supino et al. (2020) investigate a complete LFE population and not specifically repeating families. As we observed in Figure 4, an LFE population comprising seismic patches of variable size is bounded by the self-similar scaling and the unusual scaling is only observed within repeating earthquake families.

The variation of stress drop observed in natural earthquakes and the associated non self-similar scaling could also arise from other considerations. Indeed, as noted by Kaneko and Shearer (2015), rupture directivity or effects of complex geometry compared to the simplistic circular rupture model could also give rise to a variation of the earthquake moment with an almost constant corner frequency. It is also possible, as demonstrated by numerical simulations, that a fault with heterogeneous strength can lead to seismic ruptures on the same fault patch displaying variable moments but nearly constant apparent rupture size (Lin & Lapusta, 2018). Considering the diversity of these effects and their randomness, it seems quite unlikely that they all favorably contribute to producing the anomalous scaling observed across various tectonic settings. We would rather expect that such complexities produce scattering around an average value without any systematic trend. The anomalous scaling inferred from

earthquake observations has been also explained by invoking a totally different mechanism involving elastic collisions between fault gouge particles (Tsai & Hirth, 2020).

Our model is limited in several aspects. First, we simulated a 1D fault in a 2D medium; some deviations can arise compared to a rupture on a 2D fault. Our approach also requires some assumptions on the slip distribution in order to compute the potency of each rupture. However, Li et al. (2022) recently showed that numerous outcomes of 2D and 3D numerical earthquake cycle models, such as stress drop, are comparable. This supports the validity of the presented results for higher dimensions. Second, we did not incorporate the most recent advances in friction models and fault weakening mechanisms, for instance, thermal pressurization or flash weakening processes (Acosta et al., 2018; Lambert et al., 2021). We thus acknowledge that the additional physics contained in these models can give rise to results different than the ones reported here. Furthermore, we did not perform a systematic parametric study, varying the a, b and D_c parameters to test their influence on the resolved scaling. The set of parameters tested in this study has been previously considered in other simulations whose results were found stable while perturbing these values (Chen & Lapusta, 2009). Furthermore, here we only considered an isolated asperity, not interacting with any other asperities. However, faults generally contain several seismic patches that can interact and trigger each other. It remains to be investigated how these interactions can influence the properties derived in this study and impact the observed scaling, Finally, we stress that the normal stress on an asperity is not-necessarily uniform (Schmittbuhl et al., 2006). This can lead to some important effects as the change of fluid pressure on the fault can lead to a change of the contact area of the asperity and thus redistribute stress locally and modify the asperity. Here we preferred to keep a rather simple model which, despite its limitations, offers a straightforward mechanism for interpreting the variation of the moment despite similar rupture sizes observed for numerous repeating earthquake sequences worldwide. Our model proposes that these characteristics can be well understood within the framework of a frictional fault with varying average normal stress. This model requires normal stress fluctuations at the location of the asperity. The most direct explanation for such fluctuations involves the presence of fluid pressure and its variation. The existence of fluid at the location of the seismogenic patch is well understood for geothermal reservoirs but is still debated as a necessary component for the generation of low frequency earthquakes in subduction zones (Saffer & Tobin, 2011). The change of fluid pressure on the fault can then arise from a variation of the fluid pressure directly from the source region, notably in geothermal systems, or because slip on a nearby portion of the fault modifies the fluid flow and locally enhances fluid pressure (e.g., Shapiro et al., 2018).

In conclusion, our study highlights that changes in the effective normal stress can cause a significant variation of the seismic moment on a repeating earthquake sequence. This variation of the moment leads to a variation in stress drop of at most two orders of magnitude. This important fluctuation of the stress drop is observed at the transition between the seismic and aseismic slip, such that the repeating earthquake sequence exhibits a peculiar scaling behavior that can be used as an indicator of proximity to the frictional regime change.

Data Availability Statement

No data were used in this study. Version 2.3 of the software QDYN used for modeling the seismic cyle is preserved at https://doi.org/10.5281/zenodo.322459, available via GNU General Public License v3.0 only and developed openly at https://github.com/ydluo/qdyn.

Acknowledgments
We thank M. Bouchon and J. Elkhoury for discussions about the origin of the unusual scaling. We thank W. Frank and an anonymous reviewer for their corrections and suggestions. This work was carried out in the framework of the Interdisciplinary Thematic Institute GeoT, as part of the ITI 2021–2028 program of the University of Strasbourg, CNRS and Inserm. It was supported by IdEx Unistra (ANR-10-IDEX-0002), and by SFRI-STRAT'US project (ANR ANR-20-SFRI-001) under the framework of the French Investments for the Future Program.

References

Acosta, M., Passelègue, F., Schubnel, A., & Violay, M. (2018). Dynamic weakening during earthquakes controlled by fluid thermodynamics. *Nature Communications*, *9*(1), 1–9. https://doi.org/10.1038/s41467-018-05603-9

Ampuero, J.-P., & Rubin, A. M. (2008). Earthquake nucleation on rate and state faults–aging and slip laws. *Journal of Geophysical Research*, *113*(B1), B01302. https://doi.org/10.1029/2007jb005082

Barbot, S. (2019). Slow-slip, slow earthquakes, period-two cycles, full and partial ruptures, and deterministic chaos in a single asperity fault. *Tectonophysics*, *768*, 228171. https://doi.org/10.1016/j.tecto.2019.228171

Bostock, M. G., Thomas, A. M., Savard, G., Chuang, L., & Rubin, A. M. (2015). Magnitudes and moment-duration scaling of low-frequency earthquakes beneath southern vancouver island. *Journal of Geophysical Research: Solid Earth*, *120*(9), 6329–6350. https://doi.org/10.1002/2015jb012195

Bouchon, M., Karabulut, H., Aktar, M., Özalaybey, S., Schmittbuhl, J., & Bouin, M.-P. (2011). Extended nucleation of the 1999 m w 7.6 izmit earthquake. *Science*, *331*(6019), 877–880. https://doi.org/10.1126/science.1197341

Bourouis, S., & Bernard, P. (2007). Evidence for coupled seismic and aseismic fault slip during water injection in the geothermal site of Soultz (France), and implications for seismogenic transients. *Geophysical Journal International*, *169*(2), 723–732. https://doi.org/10.1111/j.1365-246x.2006.03325.x

Cauchie, L., Lengliné, O., & Schmittbuhl, J. (2020). Seismic asperity size evolution during fluid injection: Case study of the 1993 soultz-sous-forêts injection. *Geophysical Journal International*, *221*(2), 968–980. https://doi.org/10.1093/gji/ggaa051

Chaves, E., Schwartz, S., & Abercrombie, R. (2020). Repeating earthquakes record fault weakening and healing in areas of megathrust postseismic slip. *Science Advances*, *6*(32), eaaz9317. https://doi.org/10.1126/sciadv.aaz9317

Chen, T., & Lapusta, N. (2009). Scaling of small repeating earthquakes explained by interaction of seismic and aseismic slip in a rate and state fault model. *Journal of Geophysical Research*, *114*(B1). https://doi.org/10.1029/2008jb005749

Cornet, F., Helm, J., Poitrenaud, H., & Etchecopar, A. (1997). Seismic and aseismic slips induced by large-scale fluid injections. *Pure and Applied Geophysics*, *150*(3–4), 563–583. https://doi.org/10.1007/s000240050093

De Barros, L., Cappa, F., Deschamps, A., & Dublanchet, P. (2020). Imbricated aseismic slip and fluid diffusion drive a seismic swarm in the corinth gulf, Greece. *Geophysical Research Letters*, *47*(9), e2020GL087142. https://doi.org/10.1029/2020gl087142

De Barros, L., Guglielmi, Y., Rivet, D., Cappa, F., & Duboeuf, L. (2018). Seismicity and fault aseismic deformation caused by fluid injection in decametric in-situ experiments. *Comptes Rendus Geoscience*, *350*(8), 464–475. https://doi.org/10.1016/j.crte.2018.08.002

Dieterich, J. H. (1992). Earthquake nucleation on faults with rate-and state-dependent strength. *Tectonophysics*, *211*(1–4), 115–134. https://doi.org/10.1016/0040-1951(92)90055-b

Duputel, Z., Tsai, V. C., Rivera, L., & Kanamori, H. (2013). Using centroid time-delays to characterize source durations and identify earthquakes with unique characteristics. *Earth Planetary Science Letters*, *374*, 92–100. https://doi.org/10.1016/j.epsl.2013.05.024

Eshelby, J. D. (1957). The determination of the elastic field of an ellipsoidal inclusion, and related problems. *Proceedings of the Royal Society of London. Series A. Mathematical and Physical Sciences*, *241*(1226), 376–396.

Farge, G., Shapiro, N. M., & Frank, W. B. (2020). Moment-duration scaling of low-frequency earthquakes in Guerrero, Mexico. *Journal of Geophysical Research: Solid Earth*, *125*(8), e2019JB019099. https://doi.org/10.1029/2019jb019099

Frank, W. B., Radiguet, M., Rousset, B., Shapiro, N. M., Husker, A. L., Kostoglodov, V., et al. (2015). Uncovering the geodetic signature of silent slip through repeating earthquakes. *Geophysical Research Letters*, *42*(8), 2774–2779. https://doi.org/10.1002/2015gl063685

Gischig, V. S. (2015). Rupture propagation behavior and the largest possible earthquake induced by fluid injection into deep reservoirs. *Geophysical Research Letters*, *42*(18), 7420–7428. https://doi.org/10.1002/2015gl065072

Harrington, R. M., & Brodsky, E. E. (2009). Source duration scales with magnitude differently for earthquakes on the San Andreas fault and on secondary faults in Parkfield, California. *Bulletin of the Seismological Society of America*, *99*(4), 2323–2334. https://doi.org/10.1785/0120080216

Kaneko, Y., & Shearer, P. (2015). Variability of seismic source spectra, estimated stress drop, and radiated energy, derived from cohesive-zone models of symmetrical and asymmetrical circular and elliptical ruptures. *Journal of Geophysical Research: Solid Earth*, *120*(2), 1053–1079. https://doi.org/10.1002/2014jb011642

Kato, N. (2012). Dependence of earthquake stress drop on critical slip-weakening distance. *Journal of Geophysical Research*, *117*(B1). https://doi.org/10.1029/2011jb008359

Lambert, V., Lapusta, N., & Faulkner, D. (2021). Scale dependence of earthquake rupture prestress in models with enhanced weakening: Implications for event statistics and inferences of fault stress. *Journal of Geophysical Research: Solid Earth*, *126*(10), e2021JB021886. https://doi.org/10.1029/2021JB021886

Lapusta, N., & Rice, J. R. (2003). Nucleation and early seismic propagation of small and large events in a crustal earthquake model. *Journal of Geophysical Research*, *108*(B4). https://doi.org/10.1029/2001jb000793

Lengliné, O., Boubacar, M., & Schmittbuhl, J. (2017). Seismicity related to the hydraulic stimulation of grt1, Rittershoffen, France. *Geophysical Journal International*, *208*(3), 1704–1715. https://doi.org/10.1093/gji/ggw490

Lengliné, O., Lamourette, L., Vivin, L., Cuenot, N., & Schmittbuhl, J. (2014). Fluid-induced earthquakes with variable stress drop. *Journal of Geophysical Research: Solid Earth*, *119*(12), 8900–8913. https://doi.org/10.1002/2014jb011282

Li, M., Pranger, C., & van Dinther, Y. (2022). Characteristics of earthquake cycles: A cross-dimensional comparison of 0d to 3d numerical models. *Journal of Geophysical Research: Solid Earth*, *127*(8), e2021JB023726. https://doi.org/10.1029/2021JB023726

Lin, Y.-Y., & Lapusta, N. (2018). Microseismicity simulated on asperity-like fault patches: On scaling of seismic moment with duration and seismological estimates of stress drops. *Geophysical Research Letters*, *45*(16), 8145–8155. https://doi.org/10.1029/2018gl078650

Lin, Y.-Y., Ma, K.-F., Kanamori, H., Song, T.-R. A., Lapusta, N., & Tsai, V. C. (2016). Evidence for non-self-similarity of microearthquakes recorded at a taiwan borehole seismometer array. *Geophysical Journal International*, *206*(2), 757–773. https://doi.org/10.1093/gji/ggw172

Luo, Y., & Ampuero, J.-P. (2018). Stability of faults with heterogeneous friction properties and effective normal stress. *Tectonophysics*, *733*, 257–272. https://doi.org/10.1016/j.tecto.2017.11.006

Luo, Y., Ampuero, J. P., Galvez, P., van den Ende, M., & Idini, B. (2017). Qdyn: A quasi-dynamic earthquake simulator (v1.1). *Zenodo*. https://doi.org/10.5281/zenodo.322459

Miller, S. A. (2013). The role of fluids in tectonic and earthquake processes. *Advances in Geophysics*, *54*, 1–46.

Passelègue, F. X., Almakari, M., Dublanchet, P., Barras, F., Fortin, J., & Violay, M. (2020). Initial effective stress controls the nature of earthquakes. *Nature Communications*, *11*(1), 1–8. https://doi.org/10.1038/s41467-020-18937-0

Rubin, A. M. (2008). Episodic slow slip events and rate-and-state friction. *Journal of Geophysical Research*, *113*(B11), B11414. https://doi.org/10.1029/2008jb005642

Rubin, A. M., & Ampuero, J.-P. (2005). Earthquake nucleation on (aging) rate and state faults. *Journal of Geophysical Research*, *110*(B11). https://doi.org/10.1029/2005jb003686

Saffer, D. M., & Tobin, H. J. (2011). Hydrogeology and mechanics of subduction zone forearcs: Fluid flow and pore pressure. *Annual Review of Earth and Planetary Sciences*, *39*(1), 157–186. https://doi.org/10.1146/annurev-earth-040610-133408

Savage, J. (1972). Relation of corner frequency to fault dimensions. *Journal of Geophysical Research*, *77*(20), 3788–3795. https://doi.org/10.1029/jb077i020p03788

Schmittbuhl, J., Chambon, G., Hansen, A., & Bouchon, M. (2006). Are stress distributions along faults the signature of asperity squeeze? *Geophysical Research Letters*, *33*(13), L13307. https://doi.org/10.1029/2006gl025952

Scholz, C. H. (1998). Earthquakes and friction laws. *Nature*, *391*(6662), 37–42. https://doi.org/10.1038/34097

Scuderi, M. M., & Collettini, C. (2016). The role of fluid pressure in induced vs. triggered seismicity: Insights from rock deformation experiments on carbonates. *Scientific Reports*, *6*(1), 24852. https://doi.org/10.1038/srep24852

Shapiro, N. M., Campillo, M., Kaminski, E., Vilotte, J.-p., & Jaupart, C. (2018). Low-frequency earthquakes and pore pressure transients in subduction zones. *Geophysical Research Letters*, *45*(20), 11–083. https://doi.org/10.1029/2018gl079893

Supino, M., Poiata, N., Festa, G., Vilotte, J.-P., Satriano, C., & Obara, K. (2020). Self-similarity of low-frequency earthquakes. *Scientific Reports*, *10*(1), 1–9. https://doi.org/10.1038/s41598-020-63584-6

Thomas, M. Y., Lapusta, N., Noda, H., & Avouac, J.-P. (2014). Quasi-dynamic versus fully dynamic simulations of earthquakes and aseismic slip with and without enhanced coseismic weakening. *Journal of Geophysical Research: Solid Earth*, *119*(3), 1986–2004. https://doi.org/10.1002/2013jb010615

Tsai, V. C., & Hirth, G. (2020). Elastic impact consequences for high-frequency earthquake ground motion. *Geophysical Research Letters*, *47*(5), e2019GL086302. https://doi.org/10.1029/2019gl086302

Vidale, J., Ellsworth, W., Cole, A., & Marone, C. (1994). Variations in rupture process with recurrence interval in a repeated small earthquake. *Nature*, *368*(6472), 624–626. https://doi.org/10.1038/368624a0

Warren-Smith, E., Fry, B., Wallace, L., Chon, E., Henrys, S., Sheehan, A., et al. (2019). Episodic stress and fluid pressure cycling in subducting oceanic crust during slow slip. *Nature Geoscience*, *12*(6), 475–481. https://doi.org/10.1038/s41561-019-0367-x